Second-order Raman scattering in II–VI semiconductors: Relative intensities and trends

R. L. Schmidt,* K. Kunc,† M. Cardona, and H. Bilz
Max-Planck-Institut für Festkörperforschung,
Heisenbergstrasse 1, 7000 Stuttgart 80, Federal Republic of Germany
(Received 9 April 1979)

The second-order Raman spectra of ZnS, ZnSe, and ZnTe are calculated using an anharmonic overlap shell model for their lattice dynamics. These calculations are fitted to the experiments and the corresponding nonlinear polarizabilities of Zn, S, Se, and Te are derived. The systematics of these parameters are discussed. As a by-product the measured relative strengths of the first-order scattering by TO phonons are interpreted with a microscopic-deformation-potential model.

I. INTRODUCTION

During the past few years the study of the Raman scattering of zinc-blende-type semiconductors has received considerable attention.[1–5] While the first-order spectrum yields accurate values for the energies of the LO and TO phonons at $\vec{k} \simeq 0$ (Γ point) the second-order spectrum, when interpreted with the help of lattice-dynamical models,[6–8] yields the energies of a number of critical points mostly at the edge of the Brillouin zone.

Not only the location of structure in the Raman spectra but also the intensity of these structures, and with it the mechanism of the scattering process, has received interest.[1,9,10] The aim of this type of work is usually to obtain information about the first- and second-order[11,12] electron-phonon interactions. Two approaches can be followed; (i) microscopic ones, based on the electron energy bands and the deformation potentials for the electron-phonon interaction[2,5,9] and (ii) macroscopic ones, often based on lattice-dynamical shell models with anharmonic spring constants.[10,13,14] The band-structure approaches are particularly suited for treating resonance phenomena when the laser frequency lies near that of a strong energy gap.[2]

In this work we discuss the second-order Raman scattering by phonons in ZnS, ZnSe, and ZnTe. The reported independent-symmetry-component spectra are basically the same as those of Ref. 5 except that care was taken to determine the relative strengths of one material compared with the others. Away from resonance the spectra are described in terms of a nonlinear shell model first proposed by Bruce and Cowley[13] using the harmonic parameters of the overlap shell model[15] determined by Kunc and Bilz for these materials.[10] A reasonable fit of the three independent components of the second-order spectra of each compound and their relative intensities is possible using only two nonlinear ion-shell spring constants for each material (one for each of the constituent ions). The systematics of the values obtained for these parameters is discussed in the light of previous ideas concerning the polarizability of chalcogen ions. As a by-product, the relative intensities of first-order scattering by TO phonons are discussed in terms of deformation-potential theory.

II. EXPERIMENTS

The experiments were performed in the backscattering geometry on (110) and (100) surfaces using commercially available gas (Ar^+, Kr^+, N_2) and jet-stream dye lasers. The spectra were measured in the geometry that gives the symmetry combinations $\Gamma_1+\Gamma_{12}+\Gamma_{15}$, $\Gamma_1+4\Gamma_{12}$, and Γ_{15}. By digitally combining the spectra, the individual symmetry components, Γ_1, Γ_{15}, and Γ_{12}, could be obtained. As has been observed in all tetrahedral semiconductors,[2–5,9] the Γ_1 component appears most strongly while the Γ_{15} is somewhat weaker. The Γ_{12} is the weakest component of the spectra: its intensity lies below the experimental noise.

The lasers used for the determination of the relative intensities of the II–VI materials were chosen such that their wavelengths were equal to 80% (±4%) of the band gap ω_0 in all three materials ($\omega/\omega_0 \simeq 0.8$).[5] The resonance effects, already quite small, should thus be equal in all three samples. From Ref. 5 we estimate the resonance enhancement at $\omega/\omega_0 = 0.8$ to be about a factor of 2.

The intensities of the spectra were corrected for the absorption of the laser and the scattered radiation.[14] Absorption measurements on 50- and 100-μm-thick slabs, cut from the same crystals from which the Raman spectra were measured, provided an accurate means of determining the absorption coefficient for each material. Further intensity corrections due to the spectrometer and photomultiplier responsivity were performed by measuring the intensity of the

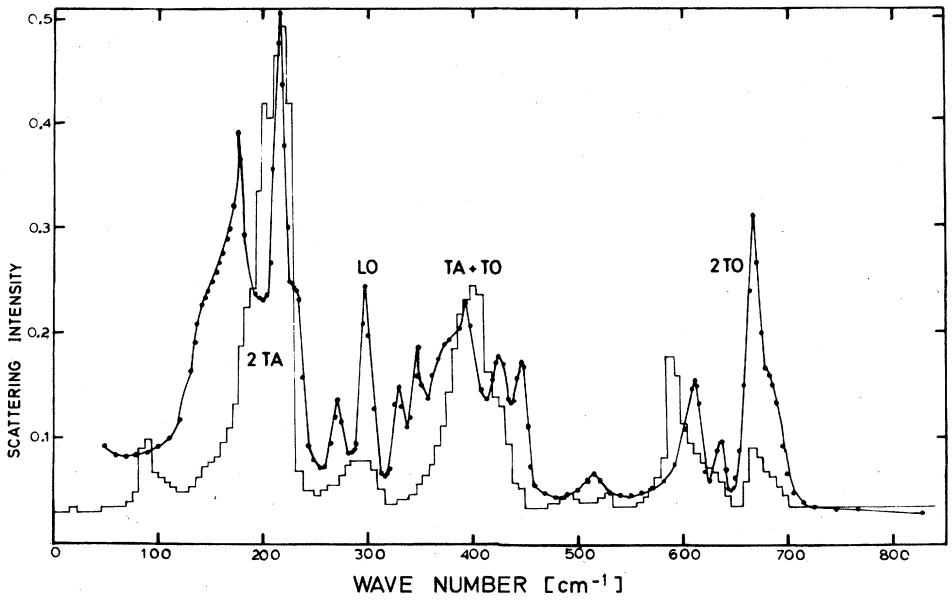

FIG. 1. Γ_1 component of the second-order Raman spectrum of ZnS measured at room temperature. Also (histogram) fit based on the anharmonic shell model described in the text with the parameters H_1(Zn) and H_1(S) given in Table I.

320-cm^{-1} phonon line of CaF_2 as a function of laser frequency. CaF_2 has a band gap of about 10 eV and, except for the well-known ω^4 factor,[1] does not show any resonance effects in our region of interest. Thus our data correctly represent the relative scattering intensities of the three materials measured divided by ω^4. They are normalized so as to make the height of the TO phonon of ZnTe in the allowed Γ_{15} configuration equal to unity.

III. RESULTS AND DISCUSSION

A. Second-order scattering

Figures 1–3 show the Γ_1 spectra of ZnS, ZnSe, and ZnTe measured at room temperature. The corresponding Γ_{15} components of ZnSe and ZnTe are displayed in Figs. 4 and 5 (that of ZnS has already been presented in Ref. 10). The Γ_{12} components are negligible as already mentioned, a fact that is also reproduced by the calculations to be discussed below. The Γ_1 components are composed mostly of TO and TA overtones with some contribution of TA + TO combinations.[5] The weak Γ_{15} components contain mainly TA + TO combinations and some 2TA overtones.

The histograms of Figs. 1–5 were obtained with the nonlinear shell-model approach.[13] The harmonic parameters of the valence overlap shell model[10] were taken from the literature (Ref. 6 for ZnS and ZnTe, Ref. 10 for ZnSe). They consist of ten adjustable parameters including five short-range interionic force constants, a shell charge Y_κ, and a shell restoring

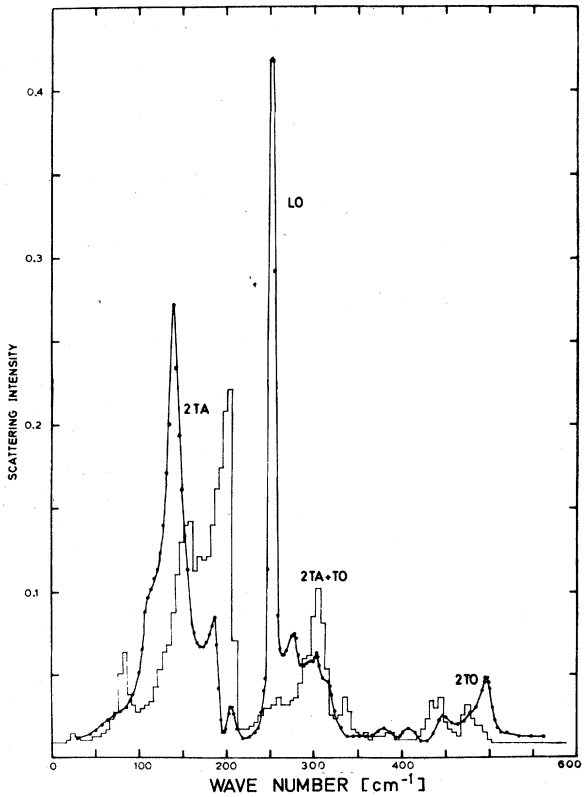

FIG. 2. Γ_1 component of the second-order Raman spectrum of ZnSe measured at room temperature. Also (histogram) fit based on the anharmonic shell model described in the text with the parameters H_1(Zn) and H_1(Se) given in Table I.

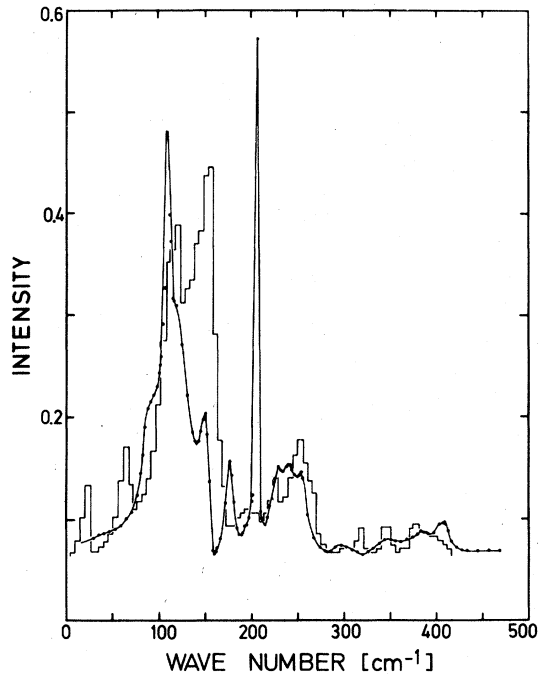

FIG. 3. Γ_1 component of the second-order Raman spectrum of ZnTe measured at room temperature. Also (histogram) fit based on the anharmonic shell model described in the text with the parameters H_1(Zn) and H_1(Te) given in Table I.

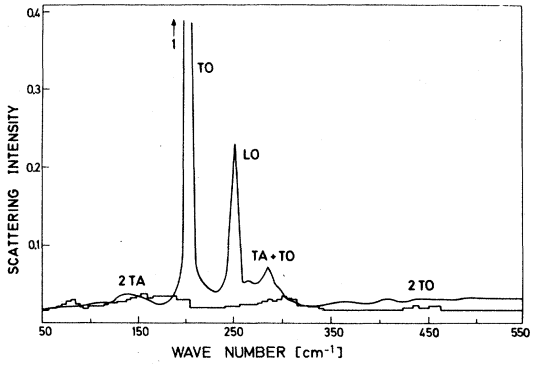

FIG. 4. Γ_{15} component of the second-order Raman spectrum of ZnSe measured at room temperature. The histogram was obtained with the theory described in the text and the same anharmonicity parameters H_1(Zn) and H_1(Se) used to fit Fig. 2.

force k_κ for each ion and an ionic charge Z. Note that the cation shell charge, Y_1, is positive in this model. The *nonlinear* interaction is defined by the potential

$$\phi^{\mathrm{NL}} = \sum_{l\kappa} H_1(\kappa) \sum_{\alpha\beta} w_\alpha^2(l\kappa)\, w_\beta^2(l\kappa) \quad . \tag{1}$$

Here $\vec{w}(l\kappa)$ are the shell displacements relative to the cores at the site $l\kappa$. The proportionality coefficient $H_1(\kappa)$ is the local nonlinear electron-ion coupling constant and the summation extends over all lattice sites and the three coordinates x,y,z. This nonlinear "spring" is superimposed on the linear spring constant k_κ, binding each shell to its own core and giving the self-energy contribution

$$\phi^{\mathrm{SE}} \simeq \tfrac{1}{2} \sum_{l\kappa} k_\kappa \sum_{\alpha} w_\alpha^2(l\kappa) \tag{2}$$

to the total shell-model potential.

The potential of Eq. (1) is ascribed to individual lattice sites, and not to bonds. Hence this approach is a *local* one and gives rise to the second-order differential polarizability (Raman tensor) $P_{\alpha\beta}(\vec{q}\,j_1, -\vec{q}\,j_2)$ [see, e.g., Ref. 16, Eq. (49.5)] in terms of a contribution from each of the two sublattices:

$$P_{\alpha\alpha}(\vec{q}\,j_1, -\vec{q}\,j_2) = -\frac{2\hbar e^2}{3v_a N} \sum_{\kappa=1}^{2} \frac{c(\kappa)^2}{(\vec{q}\,j_1)(\vec{q}\,j_2)} H_1(\kappa) \sum_{\gamma} (1+2\delta_{\alpha\gamma}) f_\gamma(\kappa|\vec{q}\,j_1) f_\gamma(\kappa|-\vec{q}\,j_2) \quad ,$$

$$P_{\alpha\beta}(\vec{q}\,j_1, -\vec{q}\,j_2) = -\frac{2\hbar e^2}{3v_a N} \sum_{\kappa=1}^{2} \frac{c(\kappa)^2}{[\omega(\vec{q}\,j_1)\omega(\vec{q}\,j_2)]^{1/2}} H_1(\kappa) [f_\alpha(\kappa|\vec{q}\,j_1) f_\beta(\kappa|-\vec{q}\,j_2) + f_\beta(\kappa|\vec{q}\,j_1) f_\alpha(\kappa|-\vec{q}\,j_2)] \quad , \tag{3}$$

where $\kappa = 1, 2$ labels the two sublattices, $\omega(\vec{q}\,j)$ is the eigenfrequency of the phonon mode $(\vec{q}\,j)$, and $\vec{f}(\vec{q}\,j)$ stands for the shell-displacement amplitude corresponding to the core-displacement eigenvector $\vec{v}(\kappa|\vec{q}\,j)$

$$\vec{f} = (S + YCY)^{-1}(T^{+} + YCZ)(M^{-1/2}\vec{v}) \tag{4}$$

(see, e.g., Ref. 17 for the established shell-model notation) and

$$c(\kappa) = \sum_{\kappa'=1}^{2} Y_{\kappa'} S^{-1}_{\alpha\alpha}(\kappa\kappa'|\vec{q}=0) \quad . \tag{5}$$

Nv_a represents the volume of the crystal.

We thus obtain the Raman tensor as the sum of two contributions, one proportional to H_1(II) and another proportional to H_1(VI), where II and VI represent the cation and the anion, respectively. The

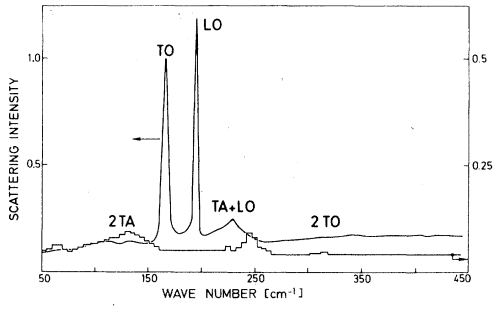

FIG. 5. Γ_{15} component of the second-order Raman spectrum of ZnTe measured at room temperature. The histogram was obtained with the theory described in the text and the same anharmonicity parameters H_1(Zn) and H_1(Te) used to fit Fig. 3.

scattering efficiency can thus be written

$$s = [H_1(\mathrm{II})R_{\mathrm{II}} + H_1(\mathrm{VI})R_{\mathrm{VI}}]^2$$
$$= H_1^2(\mathrm{II})R_{\mathrm{II}}^2 + H_1^2(\mathrm{VI})R_{\mathrm{VI}}^2 + 2H_1(\mathrm{II})H_1(\mathrm{VI})R_{\mathrm{II}}R_{\mathrm{VI}}\ , \quad (6)$$

where R are appropriate combinations of differential polarizabilities [Eq. (3)] and Bose-Einstein factors, summed over all two-phonon states. We show in Figs. 6 and 7 the calculated spectral dependences of R_{II}^2, R_{VI}^2, and $R_{\mathrm{II}}R_{\mathrm{VI}}$ for ZnS and ZnTe in arbitrary units (the same, however, in all cases and including phonon occupation numbers at room temperature). These units have been chosen so as to make the fitted value of H_1(S) (see below) equal to unity.

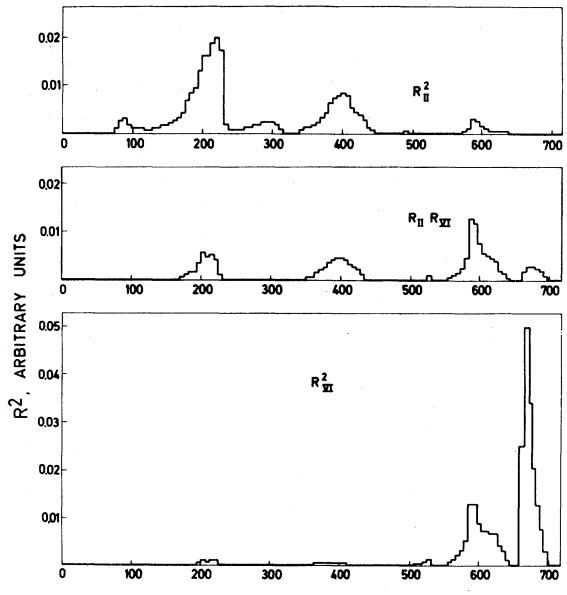

FIG. 6. Three constituent components of the calculated Γ_1 second-order Raman spectra of ZnS. The histogram of Fig. 1 is obtained by adding these components properly weighted with the anharmonicity coefficients H_1(S) and H_1(Zn) as shown in Eq. (6).

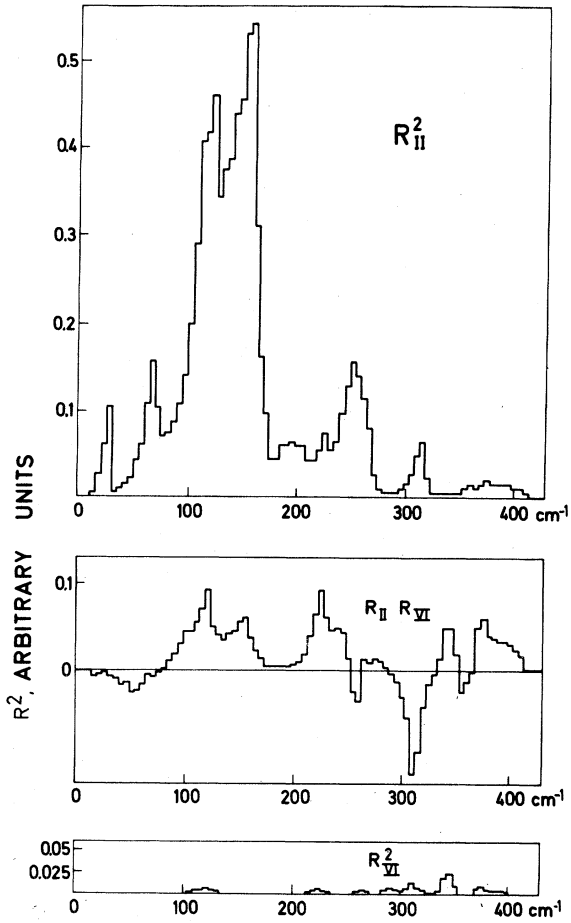

FIG. 7. Three constituent components of the calculated Γ_1 second-order Raman scattering spectra of ZnTe. The histogram of Fig. 1 is obtained by adding these components properly weighted with the anharmonicity coefficients H_1(Te) and H_1(Zn) as shown in Eq. (6).

The histograms of Figs. 1–3 were obtained as the best overall fits to the experimental data with the R_{II}^2, R_{VI}^2, and $R_{\mathrm{II}}R_{\mathrm{VI}}$ of Figs. 6 and 7 and similar data for ZnSe, by varying the anharmonic coupling constants H_1(II) and H_1(VI).

The parameters H_1 needed for the fits are listed in Table I. They seem to vary in a systematic way throughout the series of materials. Particularly obvious is the strong decrease in H_1(II) in going from ZnS to ZnTe. This decrease finds its counterpart in a strong increase of R_{II}, i.e., the highest values of R_{II} for ZnTe are one order of magnitude larger than for ZnS while those of R_{VI} are much closer, with $R_{\mathrm{S}} > R_{\mathrm{Te}}$. This fact is to be understood as a peculiarity of the lattice-dynamical model used. We note that the products $H_1(\mathrm{II})R_{\mathrm{II}}$ change by much less throughout the sequence ZnS → ZnTe. We may therefore look for an appropriate combination of parameters, instead of H_1 or R alone that is more

TABLE I. Anharmonic coupling constants H_1(II) and H_1(VI) needed for the fits of Figs. 1–3. Also, values of these parameters multiplied by $Y^2\lambda^2/k^4$. The units and values of Y, λ, and k are those of Ref. 10.

	Cation		Anion	
	H_1	$H_1\frac{Y^2\lambda^2}{k^4}$	H_1	$H_1\frac{Y^2\lambda^2}{k^4}$
ZnS	5.0	2.1×10^{11}	1.0	14.4×10^{11}
ZnSe	3.7	2.0×10^{11}	0.37	11.9×10^{11}
ZnTe	0.8	3.8×10^{11}	$\simeq$0.8	$\simeq6.8\times10^{11}$

meaningful to represent the systematics of the second-order Raman scattering. For this purpose let us note that the band-structure description of *resonant* scattering is based on the deformation potentials D_1 (for the Γ_1 component).[5] Within this description, the Stokes scattering efficiency for a given group of two phonons around a critical point is[1]

$$S \propto D_1^2 \langle u_1^2 \rangle \langle u_2^2 \rangle (1+n_1)(1+n_2) \ , \tag{7}$$

where $\langle u_i^2 \rangle$ is the zero-point average core displacement, and n_1 and n_2 are the Bose-Einstein factors of the two phonons under consideration. A comparison of Eqs. (3)–(5) with Eq. (7) indicates that D_1 (see Table II) plays approximately the same role as the following combination of shell-model parameters:

$$D_1 \sim H_1\frac{Y^2\lambda^2}{k_4}H_1\alpha^2\delta^2 \ , \tag{8}$$

with the polarizability $\alpha \simeq Y^2/k$, and the "deformability" $\delta \simeq \lambda/k$. λ is a rough representation of the matrix T, Eq. (4), by a nearest-neighbor force.[10] We have thus also listed in Table I this combination of parameters obtained from the fitted H_1(II) and H_1(VI) and the Y's and k's of Ref. 10. The systematics of these renormalized anharmonicity parameters is more reasonable than that of the H_1's. First of all, the renormalized anion parameters are higher than the cation ones, in agreement with the intuitive idea that the anion polarizability must dominate the scattering process.[5] The residual cation parameters are due to overlap effects which become important in the case of ZnTe. We note that α(II) $\simeq Y_{II}^2/k_{II}$ increases by only 15% in going from ZnS to ZnTe. The more important decrease in H_1(II) stems from the short-range deformability parameters λ and k_{II} combined into $\delta = \lambda/k$ in Eq. (8). The increase of this overlap contribution to the Raman scattering may be attributed to the bigger size of the Te^{2-} ion as compared to the S^{2-} ion which shifts the overlap center in its relative position nearer to the Zn^{2+} ion and enhances therefore the pseudo-polarizability and -deformability of the Zn^{2+} ion (refer to Ref. 15). It seems that this analysis is the first case where the effect of overlap polarization could be, at least roughly, identified in Raman scattering.

TABLE II. Electron–two-phonon deformation potentials D_1 and D_{15} for ZnTe, ZnSe, ZnS. Also calculated electron–one-phonon deformation potential d_0 of the Γ_{15} valence band (from Ref. 5).

	Mode	D_1 (eV)	D_{15} (eV)	d_0 (eV)
	2TA	575		
ZnTe	TA+LO		340	28
	TO+LO		100	
	2TO	100		
	2TA	545		
ZnSe	TA+TO		250	27
	TO+LO		260	
	2LO	510		
	2TA	1600		
ZnS	2TO	2470		25
	2LO	5700		

The systematics of the renormalized anharmonicity parameters of Table I is similar to that of the deformation potentials D_1 of Ref. 5 (see Table II); any quantitative differences are easily accounted for by the fact that the D's represent resonance parameters for the E_0 gap while the constants of Table I are average, nonresonant values. We see in Table II that D_1 for 2TA phonons is larger than for 2TO in ZnTe while the opposite is true for ZnS. This represents the fact that the TA modes of ZnTe are mostly vibrations of the heavier and more polarizable Te atom, while the opposite is true in the case of ZnS. The average values of D_1 increase from ZnTe to ZnS in a manner similar to the renormalized anharmonic constants of Table I.

B. First-order scattering

As a byproduct of this work we have measured the ratios of scattering efficiencies for the first-order scattering by TO phonons at $\omega/\omega_0 \simeq 0.8$. The results, normalized to ZnTe, are shown in Table III. This scattering efficiency can be written[1,18]

$$S \simeq 1.9\times10^{-6}\left(\frac{d_0}{\omega_0}\right)^2\frac{\omega^4[n(\Omega)+1]a_0^3}{\mu\Omega} \times F^2\left(\frac{\omega}{\omega_0}\right) \ \mathrm{cm^{-1}sr^{-1}} \ , \tag{9}$$

TABLE III. Calculated values of the scattering efficiency for first-order TO scattering at room temperature compared with experimental values of the relative scattering efficiencies of ZnS, ZnSe, and ZnTe. The experimental and theoretical values of S/ω^4 for ZnTe are normalized to those of ZnTe.

	ZnS	ZnSe	ZnTe
S (calculated)	2.6×10^{-6}	1.6×10^{-6}	1.2×10^{-6}
S/ω^4 (experiment)	0.4	1	1
S/ω^4 (calculated)	0.43	0.69	1

where, for convenience, the laser frequency ω is in eV, the lattice constant a_0 in Å, the reduced atomic mass μ in nuclear mass units, and the phonon frequency Ω in cm^{-1}. d_0 is the deformation potential for the Γ_{15} state and ω_0 is the energy gap, both in eV. The function $F(x)$ is defined as

$$F(x) = -g(x) + \frac{4\omega_0}{\Delta_0}\left[f(x) - \left(\frac{\omega_0}{\omega_{0s}}\right)^{3/2} f(x_s)\right] ,$$

$$g(x) = x^{-2}[2-(1+x)^{-1/2}-(1-x)^{-1/2}] ,$$

$$f(x) = x^{-2}[2-(1+x)^{1/2}-(1-x)^{1/2}] , \tag{10}$$

$$x = \frac{\omega}{\omega_0}, \quad x_s = \frac{\omega}{\omega_0+\Delta_0} ,$$

where Δ_0 is the spin-orbit splitting of the Γ_{15} valence state. We have evaluated the scattering efficiencies of ZnS, ZnSe, and ZnTe for $\omega/\omega_0 = 0.8$ with Eq. (9) using the deformation potentials d_0 of Table II. The resulting values are listed in Table III. In order to compare these efficiencies with the relative experimental results they must be divided by ω^4. The result of this procedure, also shown in Table III, agrees reasonably well with experiment.

*Present address: Dept. of Electrical Eng., Univ. of Pa., Philadelphia, Pa.

†Address from January 1980: Laboratoire de Physique des Solides Associé au CNRS, Tour 13, Université P. et M. Curie, 4 pl. Jussieu, 75230 Paris - Cedex 05, France.

[1]See, *Light Scattering in Solids,* edited by M. Cardona (Springer, New York, 1975), and references therein.

[2]R. Trommer and M. Cardona, Phys. Rev. B 17, 1865 (1978).

[3]J. C. Irwin and J. L. La Combe, J. Appl. Phys. 41, 1444 (1969).

[4]J. C. Irwin and J. L. La Combe, Can. J. Phys. 50, 2596 (1972).

[5]R. L. Schmidt, B. D. McCombe, and M. Cardona, Phys. Rev. B 11, 746, (1975); R. L. Schmidt and M. Cardona, in *Physics of Semiconductors,* edited by F. G. Fumi (Tipografia Marves, Rome, 1976), p. 239.

[6]N. Vagelatos, D. Wehe, and J. S. King, J. Chem. Phys. 60, 3616 (1974).

[7]K. Kunc, Ann. Phys (Paris) 8, 319 (1973).

[8]L. A. Feldkamp, G. Venkatarman, and J. S. King, Solid State Commun. 7, 1571 (1971).

[9]B. A. Weinstein and M. Cardona, Phys. Rev. B 8, 2795 (1973).

[10]K. Kunc and H. Bilz, Solid State Commun. 19, 1027 (1976); also *Proceedings of International Conference on Neutron Scattering, Gatlinburg 1976,* edited by R. M. Moon (Oak Ridge Nat. Lab., Tennesesse, 1976), p. 195.

[11]P. J. Lin-Chung and K. L. Ngai, Phys. Rev. Lett. 29, 1910 (1972).

[12]R. Zeyher, in *Light Scattering in Solids,* edited by M. Balkanski (Flammarion, Paris, 1976), p. 87.

[13]A. D. Bruce and R. A. Cowley, Ind. J. Pure Appl. Phys. 9, 877 (1971); J. Phys. C 5, 595 (1972).

[14]R. Loudon, J. Phys. (Paris) 26, 677 (1965).

[15]H. Bilz, M. Buchenau, K. Fischer, R. Haberkorn, and U. Schröder, Solid State Commun. 16, 1023 (1975).

[16]M. Born and K. Huang, *Dynamical Theory of Crystal Lattices* (Oxford University, London, 1954).

[17]S. K. Sinha, CRC Crit. Rev. Solid State Sci. 3, 273 (1973).

[18]M. Cardona, Solid State Commun. 9, 819 (1971). We use in Eq. (9) the approximation $C_0'' \simeq a_0/2\pi$.